Modeling of Ice Accretion on Wires

LASSE MAKKONEN[1]

Institute of Marine Research, Helsinki, Finland

(Manuscript received 5 May 1983, in final form 14 April 1984)

ABSTRACT

A time-dependent numerical model of ice accretion on wires, such as overhead conductors, is presented. Simulations of atmospheric icing are made with the model in order to examine the dependence of the accreted ice amount on atmospheric conditions.

The results show that in wet growth (glaze formation) under constant atmospheric conditions, the growth rate increases with time until the process changes to dry growth. In dry growth (rime formation) the growth rate typically increases with time at the beginning of the icing process, but later decreases with time when the ice deposit has grown bigger.

The effect of air temperature on the ice load turns out to be rather small for the first 24 hours of icing in typical dry growth conditions, but it is important for long-term icing. The ultimate ice load may either increase or decrease with decreasing air temperature, depending on the other atmospheric conditions and on the duration of icing. These results largely explain the difficulties encountered in estimating the formation of ice loads by simple methods using the routinely measured meteorological parameters.

1. Introduction

Atmospheric ice accretion on wires is one of the major problems in planning and constructing power transmission lines and communications networks in regions where freezing temperatures occur frequently. Damage to structures by ice loads causes huge economic losses and operational difficulties in the power industry (Bendel and Paton, 1981). On the other hand, dimensioning the structures to endure heavier ice loads rapidly increases the construction costs. Therefore, it is important to have estimates of the intensity of icing and of the maximum ice loads in different conditions in order to optimize the design of the structures.

These estimates can be obtained by collecting long time-series of observations on ice loads, and quite extensive statistics have been obtained in this way for some locations (Rudnewa, 1973). However, in most cases this is too time-consuming and laborious for practical purposes, e.g., in the planning of a power line. Therefore, indirect methods which relate the ice accretion intensity with meteorological conditions must be used. Such methods have been developed empirically by simultaneous measurements of ice accretion and meteorological parameters (McKay and Thompson, 1969; Baranowski and Liebersbach, 1977; Ahti and Makkonen, 1982), with reasonable results. However, generalization of these results is difficult because of the cross-correlations of the factors affecting the ice growth and their variation from one locality to another. Also, the large number of variables involved with the icing, some of which are difficult to measure, complicates the interpretation of the empirical observations. Theoretical modeling is needed to reveal the basic physical processes which control the rate of icing on wires.

Considerable work has already been done in describing theoretically the intensity of icing on structures (Imai, 1953; Ackley and Templeton, 1979; Lozowski *et al.*, 1983a; McComber and Touzot, 1981; and others). Recently, Makkonen (1981) presented a model which simulates both rime formation (dry growth) and glaze formation (wet growth) on stationary structures and derived some general relationships between the intensity of icing and meteorological parameters for structures of constant size and orientation. This paper presents a time-dependent model modified from the earlier model in such a way that it is particularly suitable for the simulation of wire icing, and changes in the rate of ice accretion due to the increase of the ice deposit size, as well as the variation of ice density, are included through numerical calculation.

2. Calculation of the icing intensity

The model simulates the accretion of supercooled water droplets onto a wire such as an overhead conductor. The water droplets are supposed to move horizontally in the airstream during foggy or in-cloud conditions. Ice accretion in freezing rain at low wind speeds

[1] Present affiliation: Low Temperature Laboratory, National Research Council, Ottawa, Ontario K1A 0R6, Canada.

and snow accretion are not considered, because modeling of wet snow accretion involves snow content in air and the aerodynamics of snowflakes which are poorly known, and freezing rain during low wind speeds may involve icicle formation. Freezing rain at low wind speeds and snow accretion may cause ice loads on wires, but in most regions precipitation rarely occurs in icing conditions (Ahti and Makkonen, 1982). Ice crystals mixed with supercooled water droplets may contribute slightly to ice growth (Ashworth and Knight, 1978) but this is not taken into account in the model since the amount of ice crystals in near-ground conditions is usually small. Sponginess of the ice is not considered since liquid water does not seem to be incorporated into the ice at the small liquid water contents and rotation rates relevant to wire icing in natural conditions (Lesins *et al.*, 1980). A wind direction perpendicular to the wires is assumed in the model.

On a cylindrical object the icing intensity I, i.e., the rate of increase in the mass of ice divided by the part of the surface area of the ice deposit that faces the wind (g cm^{-2} h^{-1}) can be calculated from

$$I = \frac{2}{\pi} Enwv, \tag{1}$$

where E is the collection efficiency, i.e., the ratio of the mass flow of the impinging water droplets to the mass flow that would be experienced by the surface if the droplets were not deflected in the air stream, n is the freezing fraction, i.e., the ratio of the icing intensity to the mass flow of the impinging water droplets; v is the wind speed and w the liquid water content in the air. The quantities I, E and n in Eq. (1) are the overall values for the wire (or the ice deposit). In the model the ice deposit is supposed to maintain a circular form during the icing process due to slow rotation which it experiences because of gravity as soon as the deposit grows asymmetric (Popov and Holodov, 1978; McComber, 1982) and Eq. (1) is used. On power line conductors the accreted ice deposits sometimes have an elliptical form, especially in the vicinity of the supporting structures where twisting of the wires is prevented. However, the mean deviation from circular shape is not large, as is shown by observations on Mount Washington, New Hampshire (Howe, 1982), and by data from the USSR (more than 2500 observations) (Dranevič, 1971): The ratio of the minor axis to the major axis on actual power line conductors is 0.88 for glaze and 0.82 for rime, on the average.

a. Collection efficiency

First, the collection efficiency E_m based on the median volume diameter of the droplets distribution is determined. The calculation is based on the numerical solution of Langmuir and Blodgett (1946) for the dimensionless equation of motion of a droplet in an airflow:

$$K \frac{d\mathbf{v}'_d}{d\tau} = \frac{c_d \operatorname{Re}_r}{24} (\mathbf{v}'_a - \mathbf{v}'_d), \tag{2}$$

where τ is time,

$$K = \frac{\rho_w v d^2}{9\mu D} \tag{3}$$

is the inertia parameter, c_d the droplet drag coefficient,

$$\operatorname{Re}_r = \rho_a d|\mathbf{v}_a - \mathbf{v}_d|/\mu \tag{4}$$

the droplet Reynolds number based on the droplet's relative velocity, $\mathbf{v}'_a = \mathbf{v}_a/v$ the dimensionless air velocity and $\mathbf{v}'_d = \mathbf{v}_d/v$ is the dimensionless droplet velocity. Here d is the droplet diameter, ρ_w the water density, μ the absolute viscosity of air, D the cylinder diameter and ρ_a the air density. The air velocity vector $\mathbf{v}'_a$ is obtained from the equation for the potential flow around a cylinder, and the drag coefficient c_d as a function of Re_r from the experimental data of Langmuir and Blodgett (1946). The solution of Eq. (2) may then be used to calculate the droplet trajectories from which the total collection efficiency E_m is obtained. The results of this calculation are given by Langmuir and Blodgett (1946). The empirical fit to these data, given in Appendix A, is used in the model.

The calculation of E_m as explained above is made using the median volume diameter d_m of the droplets. In natural conditions, however, the icing cloud is not monodisperse, but has a certain droplet distribution. This means that the "real" collection efficiency E should be calculated separately for each size category, and the value of E is then the sum of these collection efficiencies multiplied by the fraction of the total liquid water content represented by that size. In order to examine how well E can be approximated with E_m, various E and E_m values were calculated for three droplet size distributions and are plotted in Fig. 1. The droplet size distributions in Fig. 1 are from the measurements made in natural ground icing conditions by Bain and Gayet (1982), and cover the typical range of size distributions. Combinations of cylinder diameters in the range 1–20 cm and wind speeds in the range 10–30 m s^{-1} were used in Fig. 1; the figure shows that the error involved using E_m instead of E is negligible when E (or E_m) is high but becomes more important at low values of E. This is because with decreasing collection efficiency an increasingly large portion of the small droplets passes the cylinder without striking it. Moreover, Fig. 1 shows that for all the droplet size distributions the relationship between E and E_m can reasonably accurately be described by a single curve. The collection efficiency E calculated using the empirical equation

$$E = 0.69E_m^{0.67} + 0.31E_m^{1.67} \tag{5}$$

for the relationship in Fig. 1 (solid line) is used in the model.

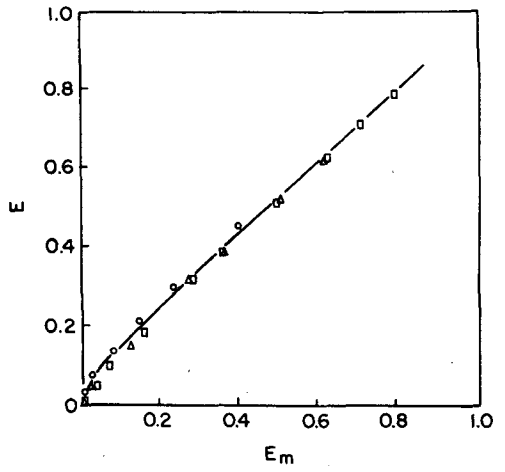

FIG. 1. Cylinder collection efficiency E calculated as a fractional sum of the collection efficiencies for each droplet size category, versus the cylinder collection efficiency E_m calculated using the median volume droplet diameter d_m. The points denoted by circles, triangles and squares are calculated for the droplet size distributions in natural icing conditions given by Bain and Gayet (1982), for d_m values of 9, 13 and 21 μm, respectively. The solid line is a best fit curve for the points [see Eq. (5)].

b. Freezing fraction

The freezing fraction in Eq. (1) can be calculated from the heat balance of the icing surface, which in this case is the front half of the cylindrical ice deposit. Accordingly, the equation for the freezing fraction becomes

$$n = \frac{\pi h}{2EvwL_f}\left[-t_a + \frac{kL_e}{c_p p_a}(e_0 - e_a) - \frac{rv^2}{2c_p}\right] - \frac{t_a}{L_f}\left(c_w + \frac{\pi\sigma a}{2Evw}\right). \quad (6)$$

The derivation of Eq. (6) is given in Appendix B and a more detailed discussion of the terms of the heat balance by Makkonen (1981).

In Eq. (6), h is the convective heat transfer coefficient, w is the liquid water content in air, L_f the latent heat of fusion at 0°C, t_a the air temperature (°C), $k = 0.62$, L_e is the latent heat of evaporation at 0°C, c_p the specific heat of air at constant pressure, p_a the air pressure, e_0 and e_a are the saturation water vapor pressures over water at 0°C and t_a, respectively, r is the overall recovery factor, c_w the specific heat of water, σ the Stefan–Boltzmann constant, and $a = 8.1 \times 10^7$ K^3.

The overall heat transfer coefficient h in Eq. (6) can be written in terms of the overall Nusselt number Nu as

$$h = \frac{k_a \mathrm{Nu}}{D}, \quad (7)$$

where k_a is the thermal conductivity of air. In the model the following parameterization for Nu is used:

$$\mathrm{Nu} = 0.032\ \mathrm{Re}^{0.85}, \quad (8)$$

where

$$\mathrm{Re} = \frac{\rho_a D v}{\mu_a} \quad (9)$$

is the cylinder Reynolds number. Equation (8) is a linear fit in the range $7 \times 10^4 < \mathrm{Re} < 9 \times 10^5$ to the data of Achenbach (1977) for the front half of his roughest test cylinder (roughness element height was 0.9 mm and the cylinder diameter 150 mm). Achenbach's (1977) data for the roughness element height of 0.9 mm show that the major part of the boundary layer on the front half of a cylinder is turbulent when $\mathrm{Re} > \sim 7 \times 10^4$. When Re decreases from this value there is a rather abrupt transition to the state where a laminar boundary layer dominates the major part of the cylinder surface, and this results in a lower overall Nusselt number. It is very difficult to simulate this transition since the range of Re in which it occurs strongly depends on the roughness element height, which is poorly known for icing surfaces. For a rougher cylinder the transition occurs at lower values of Re. Wind tunnel icing experiments (e.g., Lozowski *et al.*, 1983b) indicate that the typical roughness element height, particularly in the wet growth process, tends to be more than 0.9 mm. Hence, the overestimation of Nu (and h) at small Reynolds numbers resulting from the use of Eq. (8) in the model for the entire relevant range of Re ($1 \times 10^4 < \mathrm{Re} < 1 \times 10^6$) is probably small. If the roughness element height is much smaller than 0.9 mm the error in Nu may, however, be as much as ~70% at small Reynolds numbers.

Ice growth is considered wet in the model when $n < 1$, which means that there is some runoff from the ice deposit as a whole. This runoff water is assumed to be shed into the wind at the edges of the cylinder. In dry growth ($n = 1$) there is no runoff from the deposit. When $n = 1$ the ice growth near the stagnation line may still be wet. This, however, has no implication for the icing intensity calculated using the overall value $n = 1$, since in this case all the impinging water eventually turns into ice at some location on the cylinder surface. On the other hand, it is observed (e.g., Lozowski *et al.*, 1983b) that if $n < 1$ for the whole cylinder, then the icing process is in the wet growth regime near the stagnation line also.

3. Time dependence in the model

During the process of ice accretion on a structure, the dimensions of the ice deposit change. In the case of wire icing simulated here, this effect is restricted to the increase of the ice deposit diameter D, since the deposit is supposed to be circular during its growth due to the rotation of the wire. When the time dependence of D in Eq. (1) is taken into account and the atmospheric conditions are kept unchanged, then

$$I(\tau) = \frac{2}{\pi} E(\tau) n(\tau) v w, \tag{10}$$

and the ice load M_i per unit length of the wire at time τ_i is

$$M_i = \int_0^{\tau_i} I(\tau) \frac{\pi}{2} D(\tau) d\tau = v w \int_0^{\tau_i} E(\tau) n(\tau) D(\tau) d\tau. \tag{11}$$

The increase in D during the icing process has the following time-dependent effects on the growth of the ice load:

- Icing intensity I decreases in dry growth because of a decrease in the collection efficiency E.
- Icing intensity I decreases in wet growth because of a decrease in the heat exchange coefficient h and the freezing fraction.
- The collection area and the area for the heat exchange increase.
- The density of the accreting ice decreases in dry growth because of a decrease in the droplet impact velocity and ice surface temperature. This increases the growth rate of D in relation to the icing intensity, affecting the abovementioned time-dependent processes.

The calculation of the ice load M (kg m^{-1}) is made in a stepwise manner. For each time step i the ice load M, the icing intensity I, the ice deposit diameter D, the collection efficiency E, the freezing fraction n, the density of the accreting ice ρ and the density of the total ice deposit $\bar{\rho}$ are calculated and given as output parameters. The time step $\Delta\tau$ of 10 min is used in the calculations. Test simulations made using various time steps showed that the model is quite insensitive to the choice of $\Delta\tau$. As an example, the difference between the ice loads calculated with $\Delta\tau$ = 1 h and 10 min, respectively, is less than 3% after more than 10 h of icing under typical icing conditions. This difference is larger during the very first hours of the icing process when the increment of the deposit diameter is of the same order of magnitude as the deposit diameter itself, but in these cases the ice load is very small.

The ice load M_i where the subscript i refers to the time step, is obtained from

$$M_i = M_{i-1} + I_{i-1} \frac{\pi}{2} D_{i-1} \Delta\tau, \tag{12}$$

and the ice deposit diameter D_i from

$$D_i = \left[\frac{4(M_i - M_{i-1})}{\pi \rho_i} + D_{i-1}^2 \right]^{1/2}. \tag{13}$$

Equation (13) indicates that the ice accreted during a time step is evenly distributed on the ice deposit surface, i.e., the wire rotates more than 360° during each time step. In natural conditions this is not necessarily true, possibly causing nonsymmetric ice shapes and deviations from the calculated ice deposit diameters in the time scale of one complete wire revolution. In the long-run, however, this effect is smoothed out as shown by the observed near-circular ice deposits (Dranevič, 1971). Hence, introducing Eq. (13) into the model essentially means that the cross-sectional area of the ice deposit in the mean is assumed to be that of the cylindrical deposit having the same ice mass.

The density of the ice ρ in Eq. (13) accreted during one time step is calculated using Macklin's (1962) density parameter

$$R = \frac{-v_0 d_m}{2 t_s}, \tag{14}$$

where d_m is the median volume diameter of the droplets (μm), v_0 is the impact speed of the droplets (m s^{-1}) at the stagnation region calculated according to Langmuir and Blodgett (1946) using the median volume droplet diameter d_m, and t_s is the mean surface temperature of the ice deposit (°C). The ice density ρ (g cm^{-3}) is determined from Eq. (15) which is based on Macklin (1962) and on the measurements with a rotating cylinder in natural icing conditions by Bain and Gayet (1982):

$$\left.\begin{array}{lll} \rho = 0.11 R^{0.76} & \text{for} & R \leqslant 10 \\ \rho = R(R + 5.61)^{-1} & \text{for} & 10 < R \leqslant 60 \\ \rho = 0.92 & \text{for} & R > 60 \end{array}\right\}. \tag{15}$$

However, if ρ calculated from Eq. (15) is less than 0.10 g cm^{-3}, i.e., if $R < 0.9$, then ρ is set to 0.10 g cm^{-3} in the model. This is because ρ cannot decrease infinitely and because $\rho \approx 0.1$ g cm^{-3} seems to be the approximate lower limit for the rime density in natural conditions (Leavengood and Smith, 1968, Glukhov, 1974). The impact velocity v_0 in the density parameter R can be obtained from numerical solution of Eq. (2) (Langmuir and Blodgett, 1946); it depends on the ice deposit diameter D as well as on v and d_m. The empirical fit to the results of Langmuir and Blodgett (1946) given in Appendix A is used in the model. The mean surface temperature t_s is solved numerically from the heat balance equation of the dry growth process (for its derivation see Appendix B):

$$\frac{2}{\pi} E v w (L_f + c_w t_a - c_i t_s) = h \left[(t_s - t_a) + \frac{k L_s}{c_p p_a} (e_s - e_a) - \frac{r v^2}{2 c_p} \right] + \sigma a (t_s - t_a), \tag{16}$$

where c_i is the specific heat of ice, L_s the latent heat of sublimation at t_s, and e_a the saturation water vapor pressure with respect to ice at the temperature t_s.

The total ice deposit density $\bar{\rho}_i$ for the time step i is then obtained from

$$\bar{\rho}_i = 4M_i(\pi D_i^2 - \pi D_0^2)^{-1}, \qquad (17)$$

where D_0 is the initial wire diameter.

4. Simulation results

An example of the time-evolution of the quantities relevant to the icing process as simulated by the model is shown in Figs. 2 and 3. Input parameters typical of rather severe atmospheric icing were used in the simulation. The icing intensity I decreases rapidly with time, especially in the beginning of the icing process due to the rapid relative increase in the deposit diameter (Fig. 2). In the beginning the ice load M increases rather steadily, then approaches a limiting value above which practically no icing occurs ($E \approx 0$). This limiting value is determined by the limiting ice deposit diameter D and by the ultimate ice deposit density $\bar{\rho}$. The increase of D and the behavior of ρ and $\bar{\rho}$ are also shown in Fig. 2. Ice density in Fig. 2 begins to noticeably decrease at $\tau \approx 55$ h while the point where dry growth starts is at $\tau \approx 20$ h. The freezing fraction n in Fig. 3 increases until dry growth is reached ($n = 1$). The results demonstrate that the icing process is considerably time-dependent and that the growth regime of the icing process may change even under constant atmospheric conditions.

The curvature of the ice load growth curve changes at about $\tau = 20$ h in Fig. 2, when the change from wet growth to dry growth occurs. Other examples of the model results in terms of the growth rate of the ice load $dM/d\tau$ are shown in Fig. 4. For $t_a = -10°C$ the ice growth is dry and the ice growth rate $dM/d\tau$ increases in the beginning of the icing process, has its maximum ($d^2M/d\tau^2 = 0$) at ~12 h, and then decreases. The time τ and the ice deposit diameter D at which $d^2M/d\tau^2 = 0$ depend on the atmospheric conditions. Interestingly, however, the model results show that

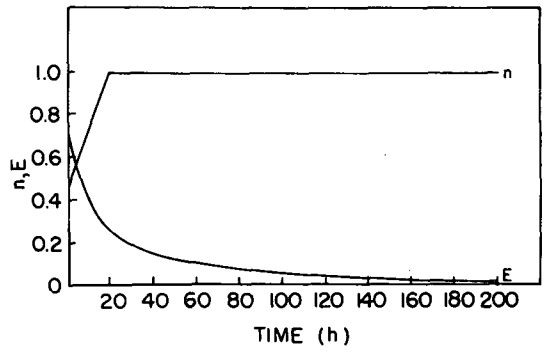

FIG. 3. Time-evolution of the freezing fraction n and the collection efficiency E, in a numerical simulation of ice accretion on a 1 cm diameter wire. Input parameters as in Fig. 2.

when $d^2M/d\tau^2 = 0$ in dry growth the collection efficiency E has the value of 0.23 irrespective of the growth conditions. This model result basically originates from the nature of the dependence of E on D and the atmospheric parameters [Eqs. (5), (A1) and (A2)]. In the wet growth regime the model shows that $dM/d\tau$ increases with time. Therefore, when the icing process starts as wet growth, the maximum icing rate occurs at the time of the transition from wet growth to dry growth unless $E > 0.23$ ($d^2M/d\tau^2 > 0$) at that time. In Fig. 4, $d^2M/d\tau^2 = 0$ at the transition for the $t_a = -1°C$ cases. The nonlinearity of the ice growth process revealed by these model results means that the duration of an icing storm becomes an important factor influencing the mean ice growth rate.

Growth curves for the ice load M for different values of the atmospheric parameters are shown in Figs. 5, 6 and 7 in order to demonstrate the sensitivity of M to variations of these parameters in storms of different duration. The sensitivity of M to the median droplet diameter d_m in Fig. 5 is high, which is unfortunate since in practical applications it is difficult to estimate the droplet size. In Fig. 6, growth curves at two wind

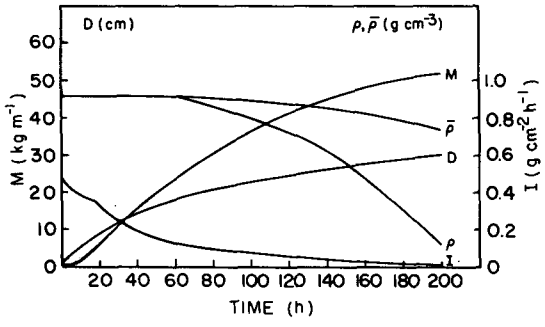

FIG. 2. Results of numerical simulation of ice accretion on a 1 cm diameter wire. The simulated quantities are ice load M, ice deposit diameter D, density of accreting ice ρ, the total deposit density $\bar{\rho}$ and the icing intensity I. Wind speed is 20 m s^{-1}, air temperature −1 °C, liquid water content 0.3 g m^{-3} and median volume droplet diameter 25 μm.

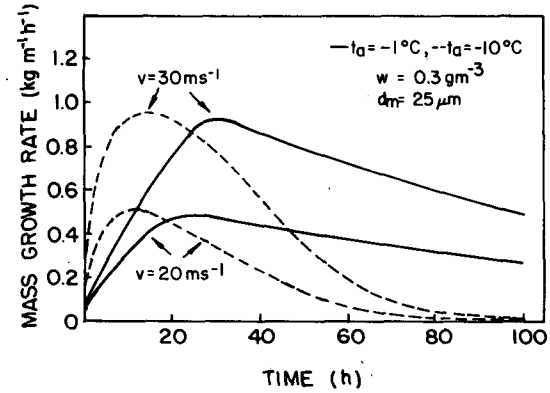

FIG. 4. Time-evolution of the growth rate of an ice load on a 1 cm diameter wire for two values of wind speed v at air temperatures $t_a = -1°C$ (solid curves), −10°C (dashed curves).

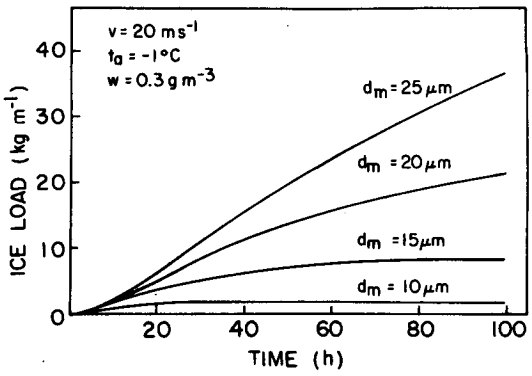

FIG. 5. Time-evolution of an ice load on a 1 cm diameter wire for various values of median volume droplet diameter d_m. The ice deposit diameter D and ice density $\bar{\rho}$ after 100 h are D = 18 cm, $\bar{\rho}$ = 0.92 g cm^{-3} for d = 25 μm; D = 19 cm, $\bar{\rho}$ = 0.80 g cm^{-3} for d = 20 μm; D = 13 cm, $\bar{\rho}$ = 0.60 g cm^{-3} for d = 15 μm; and D = 7 cm, $\bar{\rho}$ = 0.52 for d = 10 μm.

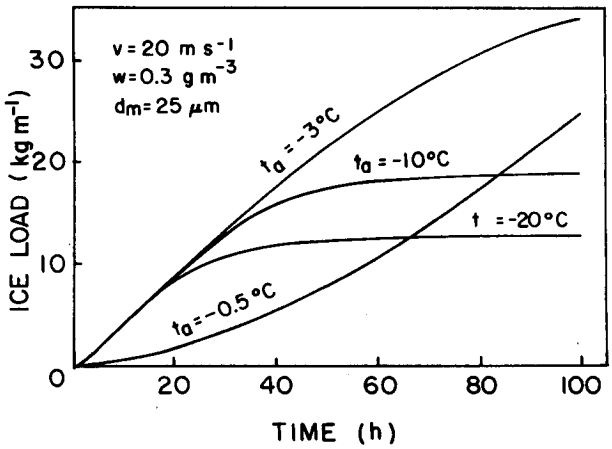

FIG. 7. As in Fig. 5 but for various values of air temperature t_a. The ice deposit diameter D and ice density $\bar{\rho}$ after 100 h are D = 28 cm, $\bar{\rho}$ = 0.56 g cm^{-3} for t_a = −3°C; D = 32 cm, $\bar{\rho}$ = 0.24 g cm^{-3} for t_a = −10°C; D = 32 cm, $\bar{\rho}$ = 0.16 g cm^{-3} for t_a = −20°C; and D = 19 cm, $\bar{\rho}$ = 0.92 g cm^{-3} for t_a = −0.5°C.

speeds for both complete dry growth (t_a = −10°C) and wet growth (t_a = −0.5°C) are shown. Figure 7 gives examples of the effect of air temperature on M. From Figs. 6 and 7, it is evident that the ratio of ice loads formed at t_a = −10°C and t_a = −0.5°C decreases with time τ. Moreover, the effect of t_a on M is such that, in general, M increases with decreasing t_a in wet growth and decreases with decreasing t_a in dry growth (Fig. 7). This can be explained qualitatively as follows. In wet growth the icing intensity I is related to the heat flux from the icing surface and this heat flux increases with decreasing t_a. In dry growth, on the other hand, t_a has no significant effect on I, but the ice density ρ decreases with decreasing t_a. Therefore, the ice deposit of a certain mass has larger dimensions when t_a is lower, and then the collection efficiency E also is smaller. As shown by the model results, for droplet sizes typical of atmospheric icing the increase in the ice deposit diameter D does not fully compensate the decrease in E in Eq. (6) if D is large ($E < 0.23$), so that the increment in the ice mass is smaller when the ice deposit is larger (t_a is lower). The relationship between M and t_a is more complicated when the growth regime changes during the icing process: In Fig. 7 the ice load M after 50 h of deposition is largest for t_a = −3°C and smallest for t_a = −0.5°C, M for t_a = −10°C being between these two values. The effect of t_a on M during pure dry growth seems to be small, except in icing storms of long duration (more than ~24 h).

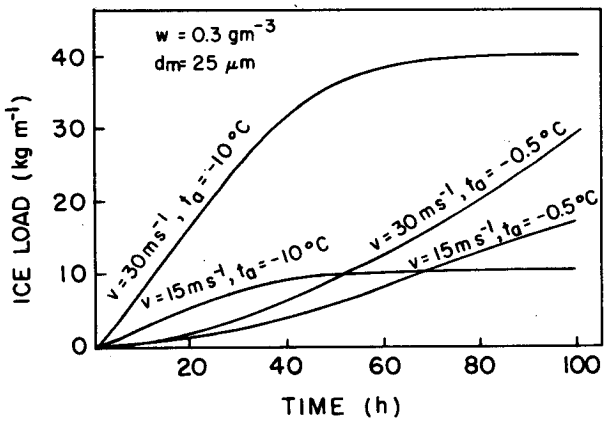

FIG. 6. As in Fig. 5 but for various values of wind speed v and air temperature t_a. The ice deposit diameter D and ice density $\bar{\rho}$ after 100 h are D = 41 cm, $\bar{\rho}$ = 0.30 g cm^{-3} for v = 30 m s^{-1}, t_a = −10°C; D = 26 cm, $\bar{\rho}$ = 0.20 g cm^{-3} for v = 15 m s^{-1}, t_a = −10°C; D = 20 cm, $\bar{\rho}$ = 0.92 g cm^{-3} for v = 30 m s^{-1}, t_a = −0.5°C; and D = 16 cm, $\bar{\rho}$ = 0.92 g cm^{-3} for v = 15 m s^{-1}, t_a = −0.5°C.

5. Discussion

The results obtained by the numerical time-dependent model show features of the ice accretion process on wires which have not been revealed by previous theoretical descriptions of icing. For example, as shown in Figs. 2 and 3 the model shows that the growth regime may change from wet growth to dry growth even under constant atmospheric conditions, and that the density of accreted ice usually decreases with time. This dependence of the ice density on the duration of icing has been observed in natural icing storms (Leavengood and Smith, 1968).

According to analytical theoretical considerations, the effect of air temperature on icing intensity is such that I is in general approximately proportional to $-t_a$ in wet growth, and there is no significant dependence on t_a in dry growth (see Makkonen, 1981). However, after a period of accretion the time-dependent model predicts that the effect of t_a on ice loads is much more complicated, as shown in Fig. 7. It is obvious that any simple formulation for the relationship between ice load M and air temperature t_a is not possible; other

atmospheric parameters influence the icing process so that M may either increase or decrease with decreasing t_a depending on v, w and d_m. This is apparently one explanation for the observed low and mostly nonsignificant correlations between M and t_a found in various studies (Ahti and Makkonen, 1982). The qualitative dependence of M on v, w and d_m predicted by the model is essentially similar to the predictions of non-time-dependent theory.

The model results show that the ice load increases nonlinearly. Hence, the ratio of the ice load calculated by a time-dependent model to the ice load calculated using the mean values of the collection efficiency E, freezing fraction n and ice deposit diameter D (see Zavarina *et al.*, 1976), depends on the duration of the icing process as well as on the growth conditions. This partly explains why in different localities the relationship between the ice load and the atmospheric parameters obtained in various studies have been slightly different. It seems that the various suggested empirical formulas relating v and M, for example, are not mutually exclusive, but can be used to describe ice accretion in storms of varying duration. For practical application of the present simulation results it may be pointed out that the mean duration of icing is ~40 h on Mt. Vitosha in Bulgaria (Stanev, 1970), while on Mt. McDill in California it is always less than 40 h, with 50% of the icing storms lasting less than 8 h (Leavengood and Smith, 1968). In the Tatras in Poland, 50% of icing events last for periods of 1–3 days (Baranowski and Liebersbach, 1977). Ice deposits do not, however, necessarily completely disappear (melt, sublimate or break off) from the wire between the icing periods, in which case longer-term simulations may be attempted.

According to the model results the growth rate of the ice load may continuously increase only when the ice deposit diameter remains small. Under more severe icing conditions the growth rate reaches its maximum value at a certain moment and then decreases. In other words, in given atmospheric conditions there is a cylinder diameter D_m which corresponds to the maximum icing rate. This diameter can be estimated by the model. Particularly in dry growth conditions, the estimation of D_m is straightforward, since the model results point out that $D = D_m$ when $E = 0.23$. This potential of the model for the optimization of structure size will be discussed in more detail in a separate article.

When comparing the results of the present model to previously suggested theoretical solutions for the estimation of wire icing, it is notable that none of the earlier formulas is able to handle an icing process which starts as wet growth and continues as dry growth. Only in the model of Imai (1953) are the two growth regimes dealt with separately. Imai's formula for glaze is essentially a simpler version of Eq. (6), including the convective heating term only (see also Kuroiwa, 1965). In the conditions typical to atmospheric icing, Imai's model gives results qualitatively similar to those of the present model. The various models of rime formation are compared in Fig. 8. The curve of Imai (1953) is based on a model where the collection efficiency E is

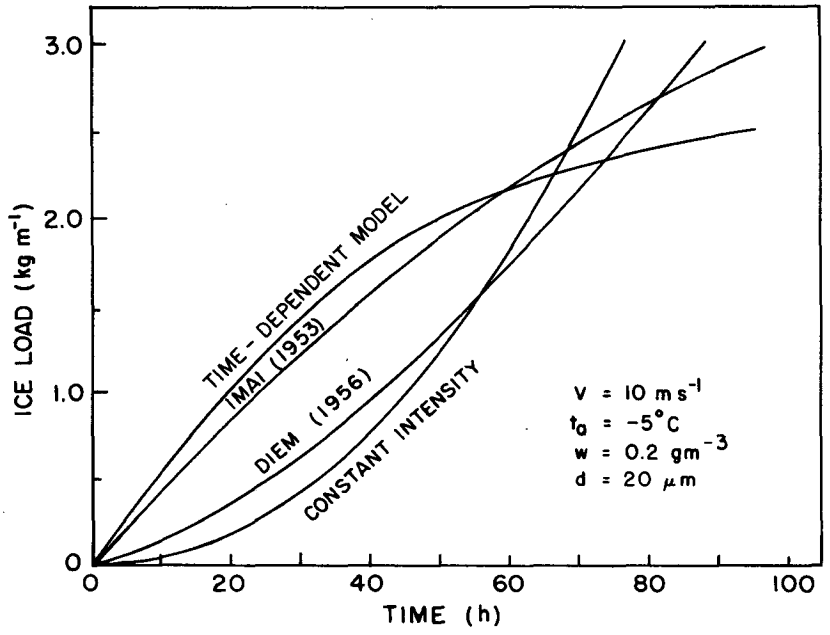

FIG. 8. Example of time-evolution of an ice load on a 0.5 cm diameter wire in a monodisperse icing cloud as calculated by different models. In the model of Imai (1953), and in the model based on constant ice intensity ($E = 0.1$), an ice density $\rho = 0.6$ g m^{-3} is assumed.

time-dependent, as in the present numerical model, but the ice density ρ is a constant (0.6 g cm^{-3}). Figure 8 shows that the present model which includes the time-dependence of ρ gives higher values of ice load M in the beginning of the icing process (for the first ~60 h), but results in smaller ultimate ice loads than Imai's model with long-term icing. A curve representing one of the empirical formulas suggested by Diem (1956),

$$M = I_0\tau^{1.4}, \quad (18)$$

where I_0 is the initial icing intensity on the noniced wire, is also shown in Fig. 8, as well as a growth curve which is based on the assumption that the icing intensity I is constant ($I = I_0$). The initial intensity I_0 for the curve by Diem (1956) and for the $I = I_0$ curve is calculated assuming that $E = 0.1$. Both the exponential growth curve and the curve based on constant I give $d^2M/d\tau^2 > 0$ for all the values of τ and are, hence, qualitatively different from the results of the present model.

The simulation results point out that observations of ice deposits on measurement instruments with long intervals of recording will not suffice to unravel the basic mechanisms determining the relationships between the icing intensity and the meteorological variables, since these relationships change with the ice deposit size and, therefore, with time. On the other hand, the time-dependence of the icing process means that short interval measurements in which the ice deposit is removed at the time of each measurement do not give representative accumulative ice loads.

The estimation of the severity of wire icing using only the routinely measured meteorological parameters will not be straightforward. Firstly, the icing intensity in dry growth is proportional to the liquid water content w, and is very sensitive to the median volume droplet diameter d_m. Neither w nor d_m are routinely measured and their estimation is difficult. Secondly, the effect of air temperature t_a and wind speed v on the ultimate ice load depends in a rather complicated way on the duration of icing and on the other growth conditions (w and d_m). As far as maximum growth rates are concerned, the estimation may be easier, since the maximum icing intensity at certain values of v and t_a is reached in wet growth, in which case ice density ρ is constant. Moreover, in the wet growth regime the effect of w and d_m on atmospheric icing rate is very small (Makkonen, 1981). However, it should be pointed out that the model results show that in typical icing conditions wet growth tends to turn to dry growth after some time of accretion even at rather high values of w and t_a, and therefore analytically calculated ice loads based on pure wet growth generally lead to overestimation of M.

It is assumed in the model that the wind direction is perpendicular to the wires, so that the angle α between the wind vector and the power line orientation, as an example, is 90°. No attempt is made in the model to take into account the effect of α being different from 90°. For practical purposes, the following equation based on the data from power line ice load measurements can be used when $\alpha \neq 90°$ (Nikiforov, 1982):

$$M(\alpha) = M(90°)[0.1 + 0.9\cos^3(90° - \alpha)]. \quad (19)$$

When applying Eq. (19) some inaccuracy is likely since the function $M = f(\alpha)$ is probably related to the growth conditions and may be different for glaze and rime, for example. In future model-building more consideration should be given to the theoretical description of the effect of α on ice load formation.

Other probable sources of error in the quantitative model results arise mainly from the possible irregularity of the ice deposit surface. The small deviation of the accretions from circular form is not likely to cause large errors because the collection efficiency (McComber and Touzot, 1981) and heat transfer (Smith *et al.*, 1983) are not very sensitive to this. However, variations in the roughness of the ice deposit surface may cause larger errors, particularly in the wet growth regime. Much more experimental work is needed to reveal the effect of the surface roughness characteristics on the heat transfer from the cylinder surface, and to determine the relationship between the degree of surface roughness and the ice growth conditions. In the dry growth regime the roughness may change the overall collection efficiency, but this effect is probably small, as shown by Macklin and Bailey (1968) for hailstones.

Turbulent wind, and sheltering by other conductors and nearby trees, etc., may also cause deviations in ice loads from theoretical predictions. Moreover, the calculation of rime density is not very accurate, particularly close to 0°C, as indicated by Macklin (1962). One reason for this is that only the droplet impact speed at the stagnation line is used in Eq. (14). There is a need for further empirical work in this area. The electric field strength on a conductor surface may also affect the ice density on power line cables (Phan and Laforte, 1981). In natural conditions, loss of ice due to ice breakage may decrease the ice load in the case of fragile, low density rime (Howe, 1982). Finally, it should be noted that the relative error in the icing rate resulting from Eqs. (A1) and (A2), and particularly from Eq. (5), may be high at very low collection efficiencies. Consequently, the droplet size distribution, in addition to the median volume diameter, must be known in order to accurately model long-term icing when the droplets are small and the wind speed is low.

In the present simulations constant atmospheric conditions have been used as input for the model. However, the model also can be used with continuously varying input parameters. Thus, more realistic results could be obtained if the typical evolution of the relevant atmospheric parameters during icing storms were used

instead of constant values. Currently, however, such observations are not available in sufficient quantity.

The main contribution of the present model is to describe *qualitatively* the physics of ice accretion on wires, and to give a conceptual framework for the development of *quantitative* estimation and prediction methods. More empirical verification is necessary in order to apply models of this kind to assess reliable design criteria for power lines, for example.

6. Conclusions

The simulation of atmospheric icing of wires by a time-dependent numerical model indicates the following:

- The growth rate of the ice load first increases and then decreases with time in dry growth (rime). The transition between these regimes occurs at the same value of the collection efficiency regardless of the growth conditions. In wet growth (glaze) the growth rate of the ice load increases with time.
- The icing process may start as wet growth and change to dry growth in constant atmospheric conditions.
- Ice density may decrease with time after dry growth conditions have been reached; this affects the growth rate of the ice load.
- The relationship between the ice load accreted and the prevailing atmospheric conditions depends strongly on the duration of the icing process.
- Decreasing air temperature may lead to either increasing or decreasing ice loads depending on the other atmospheric parameters and on the duration of icing.
- Ice load, particularly in long-term icing, is very sensitive to the droplet size in the icing fog or cloud; this hampers the estimation of icing using only the routinely measured meteorological parameters.

Acknowledgments. I wish to thank Dr. Ilkka Havukkala of the Academy of Finland, Prof. E. O. Holopainen of the Department of Meteorology, University of Helsinki, and Mr. J. R. Stallabrass of the Low Temperature Laboratory, National Research Council of Canada for their helpful comments.

This work was supported by the Vilho, Yrjö and Kalle Väisälä Foundation of the Finnish Academy of Science and Letters.

APPENDIX A

Details of the Collection Efficiency and Droplet Impact Speed Calculation

The formulas for calculating the overall collection efficiency E_m and the droplet impact speed v_0 at the stagnation line are based on the tabulated results of Langmuir and Blodgett (1946). The following fits to their numerical data are used in the model:

$$\left.\begin{aligned} E_m &= 0.5[\log(8K_0)]^{1.6} \quad \text{for} \quad K_0 \leqslant 0.8 \\ E_m &= K_0^{1.1}(K_0^{1.1} + 1.426)^{-1} \quad \text{for} \quad K_0 > 0.8 \end{aligned}\right\}, \quad \text{(A1)}$$

where

$$K_0 = K[0.087\ \mathrm{Re}_d^{(0.76\mathrm{Re}_d^{-0.027})} + 1]^{-1}. \quad \text{(A2)}$$

Equation (A2) is from Cansdale and McNaughtan (1977). Here K is the inertia parameter defined in Eq. (3) and Re_d the droplet Reynolds number based on the free stream velocity v:

$$\mathrm{Re}_d = \rho_a d v/\mu. \quad \text{(A3)}$$

For the droplet impact speed v_0 the formulas

$$\left.\begin{aligned} v_0 &= v(-0.174 + 1.464K_0 - 0.816K_0^2) \\ &\qquad \text{for} \quad K_0 \leqslant 0.55 \\ v_0 &= v[0.561 + 0.592 \log K_0 - 0.26(\log K_0)^2] \\ &\qquad \text{for} \quad K_0 > 0.55 \end{aligned}\right\}, \quad \text{(A4)}$$

where K_0 is determined from Eq. (A2), are used.

A comparison between the results obtained using Eqs. (A1) and (A4) and the data of Langmuir and Blodgett (1946) shows differences of less than 0.03 for E_m and 10% for v_0 in the range of conditions in which considerable rime icing on wires occurs ($1 < D < 50$ cm, $5 < v < 30$ m s^{-1}, $10 < d_m < 30$ μm).

APPENDIX B

Derivation of the Heat Balance Equations (6) and (16)

The heat balance equation for the icing surface is

$$q_f + q_v + q_k + q_a = q_c + q_e + q_l + q_s + q_i, \quad \text{(B1)}$$

where:

- q_f latent heat released during freezing;
- q_v frictional heating of air;
- q_k kinetic energy of the impinging water;
- q_a heat released in cooling the ice from its freezing temperature (0°C) to the surface temperature t_s;
- q_c loss of sensible heat to air;
- q_e heat loss due to evaporation (wet growth) or sublimation (dry growth);
- q_l heat loss in warming the impinging water to 0°C;
- q_s heat loss due to radiation; and
- q_i heat loss into the ice due to conduction.

The terms in (B1) can be parameterized as shown in Eqs. (B2)–(B8):

$$q_f = IL_f, \quad \text{(B2)}$$

where I is the intensity of accretion (mass per unit

time and unit area) and L_f the latent heat of fusion at 0°C;

$$q_v = \frac{hrv^2}{2c_p}, \tag{B3}$$

where h is the convective heat transfer coefficient, r the recovery factor for viscous heating ($r = 0.79$ is assumed), v the wind velocity, and c_p the specific heat of air at constant pressure; the kinetic energy of the droplets q_k can safely be neglected on stationary objects under natural atmospheric conditions;

$$q_a = Ic_i(0°C - t_s), \tag{B4}$$

where c_i is the specific heat of ice and t_s is the temperature of the surface (°C)

$$q_c = h(t_s - t_a), \tag{B5}$$

where t_a is the air temperature (°C);

$$q_e = \frac{hkL_e}{c_p p_a}(e_s - e_a), \tag{B6}$$

where $k = 0.62$, L_e is the latent heat of evaporation (or sublimation) at t_s, e_s and e_a are the saturation vapor pressures over the surface at t_s and t_a, respectively, and p_a is the free atmospheric pressure;

$$q_l = \frac{2}{\pi} Evwc_w(0°C - t_a), \tag{B7}$$

where c_w is the specific heat of water, and it is assumed that the temperature of the droplets in the free stream is the same as that of air;

$$q_s = \sigma a(t_s - t_a), \tag{B8}$$

where σ is the Stefan–Boltzmann constant and $a = 8.1 \times 10^7$ K^3. Equation (B8) is obtained by linearizing the equation for the difference in the longwave radiation emitted by the icing surface and the fog. The heat conductivity of ice is sufficiently low that q_i on a slowly rotating cylindrical ice deposit can be neglected, except in the initial stage of icing where the thickness of the ice layer is only a few millimeters.

In the wet growth process the temperature of the surface $t_s = 0$°C in Eqs. (B4)–(B6) and (B8). Therefore, q_a disappears and $e_s = e_0$ in Eq. (B6), where e_0 is the saturation water vapor pressure over water at 0°C. Then, using the parameterizations in Eq. (B1), neglecting q_k and q_i, and solving the icing intensity I, we obtain

$$I = hL_f^{-1}\left[-t_a + \frac{kL_e}{c_p p_a}(e_0 - e_a) - \frac{rv^2}{2c_p}\right] - L_f^{-1}\left(\frac{2}{\pi} Evwc_w + \sigma a\right)t_a. \tag{B9}$$

On combining Eqs. (1) and (B9) and solving the freezing fraction n, Eq. (6) is obtained.

In the dry growth process the temperature of the surface $t_s < 0$°C. The surface is then in the ice phase and, therefore, e_s in Eq. (B6) is the saturation water vapor pressure over ice at t_s, and L_e is the latent heat of sublimation at t_s. Again using the parameterizations (B2)–(B8), rearranging the terms, and taking Eq. (1) into account ($n = 1$ in dry growth), the heat balance given in Eq. (16) is obtained.

REFERENCES

Achenbach, E., 1977: The effect of surface roughness on the heat transfer from a circular cylinder to the cross flow of air. *Int. J. Heat Mass Transf.*, **20**, 359–369.

Ackley, S. F., and M. K. Templeton, 1979: Computer modeling of atmospheric ice accretion. Rep. 79-4, U.S. Army Cold Regions Res. Eng. Lab., Hanover, NH, 36 pp.

Ahti, K., and L. Makkonen, 1982: Observations on rime formation in relation to routinely measured meteorological parameters. *Geophysica*, **19**, 75–85.

Ashworth, T., and C. A. Knight, 1978: Cylindrical ice accretions as simulations of hail growth. I: Effects of rotation and mixed clouds. *J. Atmos. Sci.*, **35**, 1987–1996.

Bain, M., and J. F. Gayet, 1982: Contribution to the modeling of the ice accretion process: Ice density variation with the impact surface angle. *Ann. Glaciol.*, **4**, 19–23.

Baranowski, S., and J. Liebersbach, 1977: The intensity of different kinds of rime on the upper tree line in the Sudety mountains. *J. Glaciol.*, **19**, 489–497.

Bendel, W. B., and D. Paton, 1981: A review on the effect of ice storms on the power industry. *J. Appl. Meteor.*, **20**, 1445–1449.

Cansdale, J. T., and I. I. McNaughtan, 1977: Calculation of surface temperature and ice accretion rate in a mixed water droplet/ice crystal cloud. Tech. Rep. 77090, Royal Aircraft Establishment, Farnborough, U.K., 29 pp.

Diem, M., 1956: Ice loads on high voltage conductors in the mountains. *Arch. Meteor. Geophys. Bioklim.*, **B7**, 84–95 (in German).

Dranevič, E. P., 1971: *Glaze and Rime. Gidrometeorologitsheskoe Izdatelstvo*, Leningrad, 227 pp. (in Russian).

Glukhov, V. G., 1974: Distribution of glaze-rime deposits in the lower 300-meter layer of the atmosphere. AD785965, U.S. Army Foreign Sci. Tech. Center Transl., 18 pp.

Howe, J. B., 1982: Measurements and analysis of icing and wind loads on wires. Final rep., U.S. Army Cold Regions Res. Eng. Lab., Hanover, NH, 8 pp.

Imai, I., 1953: Studies of ice accretion. *Res. Snow Ice*, **1**, 35–44 (in Japanese).

Kuroiwa, D., 1965: Icing and snow accretion on electric wires. Rep. 123, U.S. Army Cold Regions Res. Eng. Lab., Hanover, NH, 10 pp.

Langmuir, I., and K. B. Blodgett, 1946: A mathematical investigation of water droplet trajectories. Tech. Rep. 5418, USAAF, 65 pp.

Leavengood, D. C., and T. B. Smith, 1968: Studies on transmission line icing. Rep. MRI68 FR-801, Meteorology Research Inc., Altadena, CA, 42 pp.

Lesins, G. B., R. List and P. I. Joe, 1980: Ice accretions, Part I: Testing of new atmospheric icing concepts. *J. Rech. Atmos.*, **14**, 347–356.

Lozowski, E. P., J. R. Stallabrass and P. F. Hearty, 1983a: The icing of an unheated, nonrotating cylinder. Part I: A simulation model. *J. Climate Appl. Meteor.*, **22**, 2053–2062.

——, —— and ——, 1983b: The icing of an unheated, nonrotating cylinder. Part II: Icing wind tunnel experiments. *J. Climate Appl. Meteor.*, **22**, 2063–2074.

Macklin, W. C., 1962: The density and structure of ice formed by accretion. *Quart. J. Roy. Meteor. Soc.*, **88,** 30–50.

——, and I. H. Bailey, 1968: The collection efficiencies of hailstones. *Quart. J. Roy. Meteor. Soc.*, **94,** 393–396.

Makkonen, L., 1981: Estimating intensity of atmospheric ice accretion on stationary structures. *J. Appl. Meteor.*, **20,** 595–600.

McComber, P., 1982: Numerical simulation of ice accretion on cables. Special Rep. 83-17, U.S. Army Cold Regions Res. Eng. Lab. Hanover, NH, 51–57.

——, and G. Touzot, 1981: Calculation of the impingement of cloud droplets in a cylinder by the finite-element method. *J. Atmos. Sci.*, **38,** 1027–1036.

McKay, G. A., and H. A. Thompson, 1969: Estimating the hazard of ice accretion in Canada from climatological data. *J. Appl. Meteor.*, **8,** 927–935.

Nikiforov, Eu. P., 1982: Icing related problems, effect of line design and ice mapping. Special Rep. 83-17, U.S. Army Cold Regions Res. Eng. Lab., Hanover, NH, 239–245.

Phan, C. L., and J.-L. Laforte, 1981: The influence of electro-freezing on ice formation on high-voltage dc transmission lines. *Cold Regions Sci. Tech.*, **4,** 15–25.

Popov, N. I., and V. V. Holodov, 1978: On the representativeness of glaze-rime observations. *Tr. Gl. Geofiz. Observ.*, **408,** 27–37 (in Russian).

Rudnewa, A. W., 1973: A climatological investigation of glaze and rime phenomena in the USSR. *Abh. Meteor. Dienst. DDR,* **107,** 10–15 (in German).

Smith, M. E., R. V. Arimilli and E. G. Keshock, 1983: Measurement of local convective heat transfer coefficient of four ice accretion shapes. Final Tech. Rep., Part I, Dept. Mech. Aerospace Eng., University of Tennessee, 95 pp.

Stanev, Sv., 1970: Ice accretion on overhead conductors in mountain conditions. *Z. Meteor.*, **20,** 161–164 (in German).

Zavarina, M. V., V. G. Glukhov and M. N. Mytariev, 1976: A method for the calculation of ice loads on high constructions. *Z. Meteor.*, **26,** 98–104 (in German).